J Mol Model (2013) 19:1027–1037
DOI 10.1007/s00894-012-1630-x

ORIGINAL PAPER

Probing mechanism of metal catalyzed hydrolysis of Thymidylyl (3′-O, 5′-S) thymidine phosphodiester derivatives

Mahboobeh Rahimian · Shridhar P. Gejji

Received: 29 March 2012 / Accepted: 3 October 2012 / Published online: 1 November 2012

Abstract Hydrolysis of nucleic acids is of fundamental importance in biological sciences. Kinetic and theoretical studies on different substrates wherein the phosphodiester bond combined with alkyl or aryl groups and sugar moiety have been the focus of attention in recent literature. The present work focuses on understanding the mechanism and energetics of alkali metal (Li, Na, and K) catalyzed hydrolysis of phosphodiester bond in modeled substrates including Thymidylyl (3′-O, 5′-S) thymidine phosphodiester (Tp-ST) *(1)*, 3′-Thymidylyl (1-trifluoroethyl) phosphodiester (Tp-OCH_2CF_3) *(2)*, 3′-Thymidylyl (o-cholorophenyl) phosphodiester (Tp-OPh(o-Cl)) *(3)* and 3′-Thymidylyl(p-nitrophenyl) phosphodiester (Tp-OPh(p-NO_2)) *(4)* employing density functional theory. Theoretical calculations reveal that the reaction follows a single-step (A_ND_N) mechanism where nucleophile attack and leaving group departure take place simultaneously. Activation barrier for potassium catalyzed Tp-ST hydrolysis (12.0 kcal mol^{-1}) has been nearly twice as large compared to that for hydrolysis incorporating lithium or sodium. Effect of solvent (water) on activation energies has further been analyzed by adding a water molecule to each metal ion of the substrate. It has been shown that activation barrier of phosphodiester hydrolysis correlates well with basicity of leaving group.

Keywords Activation barrier · A_ND_N mechanism · Density functional · Phosphodiester

Introduction

Phosphodiester bonds are known to make up the backbone of RNA or DNA strands and hence understanding hydrolysis of phosphodiester bond at the molecular level is of fundamental importance in nucleic acid chemistry. Underlying mechanism of such hydrolysis whether it involves a one step or two step process has not yet been known exactly. A one step mechanism involves a (A_ND_N) process in which bond making and breaking of P−O bond occurs simultaneously and the reaction passes through a single transition state structure without any intermediate. On the other hand, a two step mechanism can be visualized through More-O'Ferrall-Jencks diagram [1, 2]. A dissociative reaction proceeds either with cleavage of the leaving group which precedes the formation of a new phosphorus nucleophile bond usually referred to as (D_N+A_N) mechanism or an associative (A_N+D_N) mechanism in which no significant bond cleavage during the bond formation was also noticed for phosphodiester bond in different chemical environments.

DNA or RNA hydrolysis has been investigated by employing theoretical methods with the use of dimethyl and ethylene phosphates as model compounds. Dejaegere, Lim and Karplus [3] carried out theoretical calculations on base catalyzed hydrolysis of ethylene and dimethyl phosphate which revealed the reaction in gas phase proceeds through a single step mechanism without any dianionic pentacordinate intermediate. Pursuant to this ab initio calculations due to Lim and co-workers [4–8] pointed out that hydrolysis of phosphate esters and phosphodiesters proceed

Electronic supplementary material The online version of this article (doi:10.1007/s00894-012-1630-x) contains supplementary material, which is available to authorized users.

M. Rahimian · S. P. Gejji (✉)
Department of Chemistry, University of Pune,
Pune 411007, India
e-mail: spgejji@chem.unipune.ac.in

through dianionic pentacoordinated phosphorus intermediate on the reaction path which is only marginally stable. Quantum chemical HF/3-21+G(d) calculations supported a pentacovalent transition state during dimethyl phosphate hydrolysis [9].

On the experimental side investigations on these model compounds point to possibilities where a two-step pathway via a pentacoordinate intermediate or a concerted one-step pathway governed by pK_a value of the leaving group [10–12]. A gradual change of reaction mechanism of different phosphoesters was shown to be dependent on several factors including nature of the leaving group and effect of environment. Alkaline hydrolysis of DNA was investigated by Takeda et al. [13] using a variety of modeled compounds containing Thymidylyl (3′–5′) thymidine phosphodiester (Tp-OT) and those combining phosphodiester functionality with sugar or alkyl/aryl groups. In particular these authors analyzed how the nature of leaving group with varying basicity (displayed in Fig. 1) influences rate of alkaline hydrolysis in these molecular systems. These experiments clearly showed that Tp-ST hydrolyzes faster than Tp-OT. It has been conjectured that thio-substitution for oxygen around the central phosphorous does not significantly influence the electrophilicity of P atom and the enhanced hydrolysis rate of Tp-ST stems from different pK_a values reflecting better leaving ability of R-SH and R-OH substituents. It was further revealed that substrates with aryl groups hydrolyzed more rapidly than Tp-OT. Interestingly phosphodiester hydrolysis with enzyme as catalyst incorporating different metal ions is reported.

Theoretical studies on DNA and RNA hydrolysis carried out using ethylene and dimethyl phosphodiester as model systems until recently. Kinetics of phosphate ester hydrolysis catalyzed by transition metal [14–22] or lanthanide complexes [23–27] are investigated. Surprisingly the role of alkali metal ions which are cofactors in hydrolytic and other metal enzymes [28–34] has not yet been clear. It has been believed that alkali metal ions which lack low-lying empty orbitals do not coordinate to substrate or transition state. Kamerlin and Wilkie [35] analyzed role of metal ion(s) in phosphoric acid hydrolysis employing the 6–31++G** basis set. These authors concluded that associate mechanism incorporating two metal ions is favored in this case. To this end, Gejji et al. [36] employed density functional calculations for understanding the role of alkali metal as motif in methyl phosphodiester (MPDE) hydrolysis. In depth analysis of MPDE hydrolysis pathways incorporating one or two metal ions has been presented. The calculations led to the conclusion that catalysis coordinating to two alkali metal ions along the reaction path is favored. The pathways incorporating one alkali metal ion on the other hand, resulted in either very large activation barrier or either the transition state(s) or intermediate can not be identified on the potential

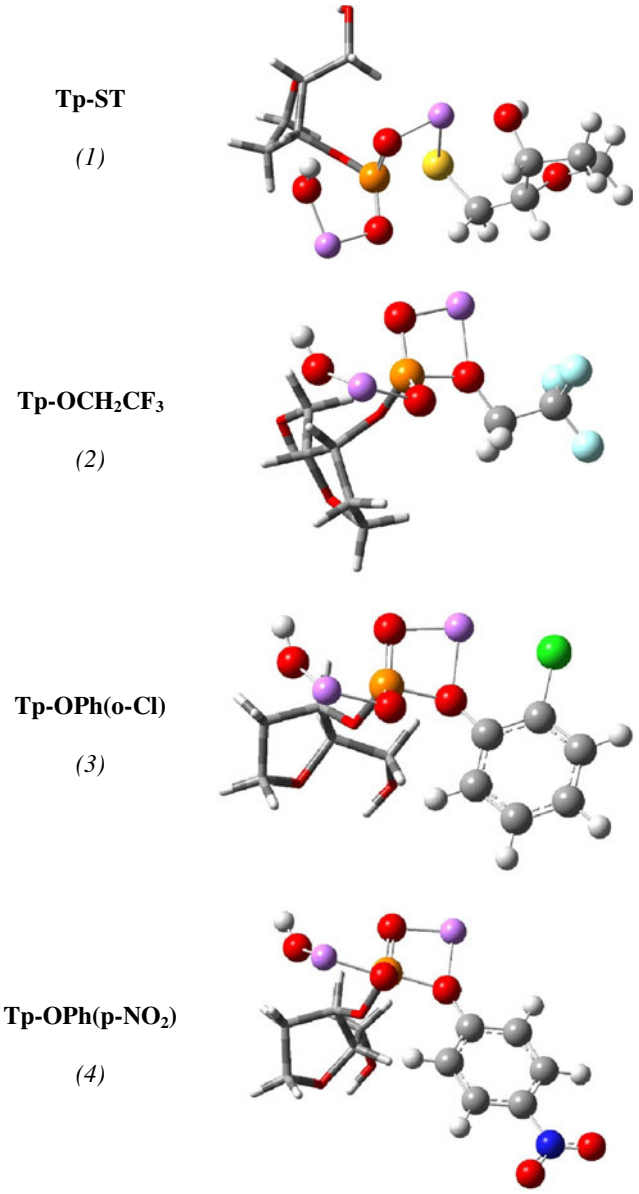

Fig. 1 Substrates (*1*−*4*) possessing varying leaving groups

energy surface. Recent studies on Tp-OT [37] supported these inferences.

The present work aims at deriving molecular insights on hydrolysis of Tp-ST derivatives with minimized perturbation around the P center (Fig. 1) and addresses the following questions: How substitution at different sites in Tp-OT influences mechanism of phosphodiester hydrolysis? How the nature of leaving group influences the energy barrier of the reaction? Moreover an interesting question which arises in metal ion catalysis in phosphodiester hydrolysis refers to whether the catalytic activity of a metal ion and hence the energy barrier of the phosphodiester hydrolysis can be improved by transferring it into a better solvating medium other than water [38]. The computational method employed in the present work is outlined below.

Computational methods

Atomic numbering scheme in Tp-ST has been shown in Fig. 2. Geometry optimizations of substrates (*1−4)* possessing varying leaving groups, two metal (Li, Na, K) ions in each case, were carried out within the framework of density functional theory that incorporated the Beck's three parameters exchange with Lee, Yang and Parr's (B3LYP) correlation functional [39, 40] using Gaussian-09 program [41]. The density functional calculations using the B3LYP functional have widely been used and generally produce very good results. Benchmarking studies on a variety of density functionals have been carried out by Ramos and coworkers [42]. These authors demonstrated that density functional calculations incorporating B3LYP functional binding energies and barrier heights in transition state reactions are well reproduced. The internally stored 6–31++G(d,p) basis set with diffuse functions being added to all non-hydrogen as well as hydrogen atoms was used in the present computations. Pathways incorporating two alkali metal ions which coordinate to phosphoester in which (i) one metal ion interact with nucleophile OH^- while other metal ion bound to either sulfur or oxygen of leaving group (**'A'** pathway) or (ii) metal ions are attached to different oxygens of phosphoryl group (**'B'** pathway) are depicted in Fig. 3. The stationary point geometries corresponding to reactants and products were confirmed to be local minima for which all normal

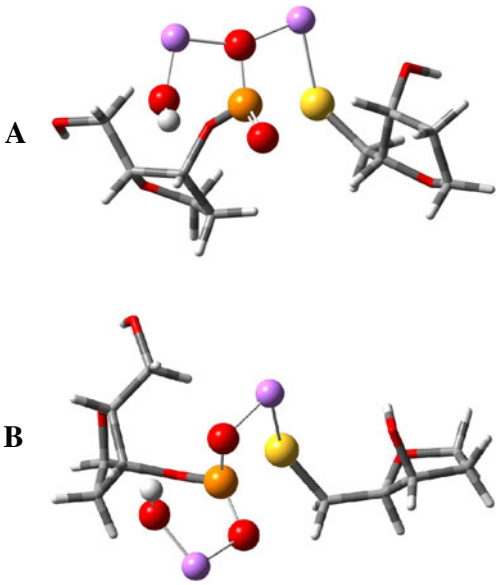

Fig. 3 Mechanistic pathways **'A'** Both metal ions interacting with single oxygen of phosphoryl group and with either the hydroxyl or 5′-S-thymidine group in Tp-ST, **'B'** both metal ions interacting with two different oxygens of phosphoryl group and with either hydroxyl or 5′-S-thymidine group of Tp-ST

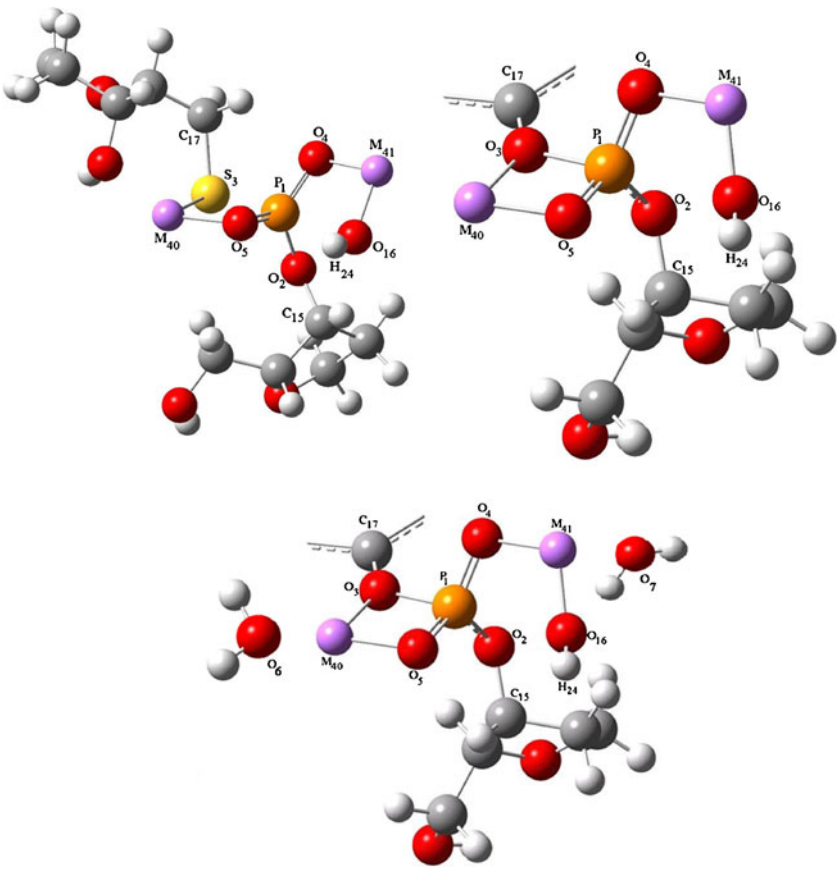

Fig. 2 Atomic numbering scheme in Tp-ST structure and other substrates

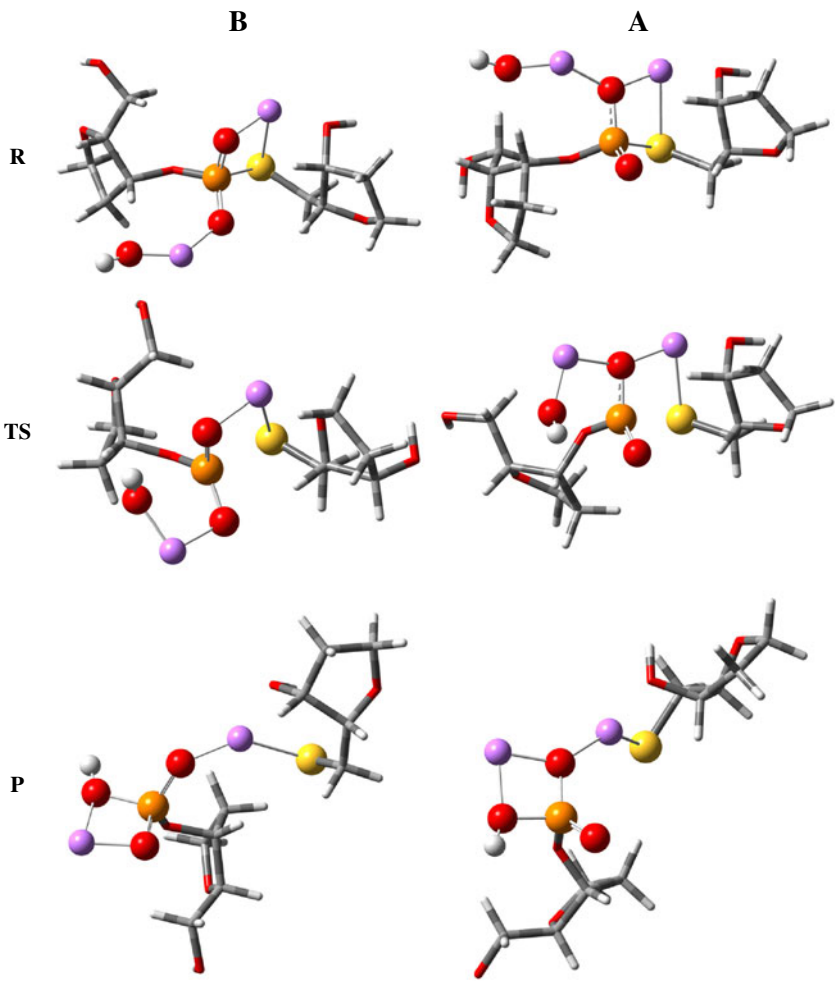

Fig. 4 Reaction profiles **'A'** and **'B'** pathway and stationary point structures in Li-catalyzed Tp-ST hydrolysis

vibration frequencies turn out to be real. An energy profile for reaction path was obtained by optimizing reactant structure as a function of nucleophile (hydroxyl ion) separation from the reaction center, which was scanned in the interval of 0.025 Å. Thus, P_1O_{16} and P_1O_3 distances respectively, refer to bond formation and bond cleavage owing to departure of leaving group. The maximum on energy profile thus obtained on subsequent optimization yields one transition state (saddle point with one imaginary frequency) structure. Effect of solvation on the stationary point structures was simulated by explicit hydration with each metal in (*1–4*) bound to a water molecule. Net atomic charges were obtained from population analyses based on the Hirshfeld partitioning scheme [43, 44].

Table 1 Activation energies (E_A) and reaction energies (E_R) in kcal mol^{-1} along **'A'** and **'B'** pathways for metal (Li, Na or K) catalyzed Tp-ST hydrolysis

	A	B		
Species	Li	Li	Na	K
E_A	8.2	6.4	9.5	12.0
E_R	−11.0	−8.7	−18.6	−32.1

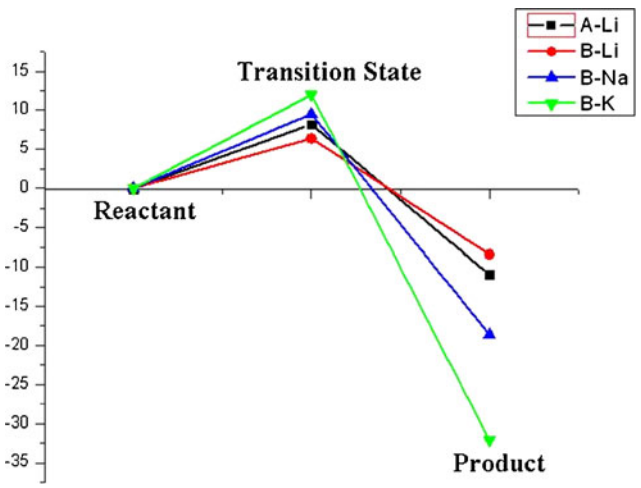

Fig. 5 Energies (in kcal mol^{-1}) of stationary point structures relative to reactant of metal catalyzed Tp-ST hydrolysis along **'A'** and **'B'** pathways

Table 2 B3LYP/6–31++G(d, p) geometrical parameters (bond lengths in Å and bond angles in °) of reactant, transition state, and product along **'A'** and **'B'** pathways for Li, Na and K catalyzed Tp-ST hydrolysis

Parameter	A			B								
	Li			Li			Na			K		
	R	TS	P	R	TS	P	R	TS	P	R	TS	P
P_1 S_3	2.172	2.315	4.544	2.173	2.286	4.719	2.179	2.313	4.919	2.204	2.362	6.022
P_1O_{16}	4.067	2.391	1.707	4.044	2.358	1.688	4.087	2.333	1.682	4.959	2.274	1.699
P_1O_4	1.570	1.576	1.552	1.531	1.538	1.502	1.526	1.529	1.506	1.520	1.525	1.506
P_1O_5	1.494	1.496	1.484	1.515	1.532	1.524	1.514	1.523	1.519	1.503	1.511	1.509
P_1O_2	1.603	1.618	1.603	1.605	1.626	1.605	1.619	1.637	1.621	1.658	1.662	1.626
S_3M_{40}	2.467	2.360	2.277	2.557	2.409	2.333	2.863	2.719	2.692	3.240	3.086	3.142
$O_{16}M_{41}$	1.652	1.701	1.882	1.666	1.725	1.950	2.038	2.080	2.306	2.387	2.441	2.713
O_4M_{40}	1.849	1.842	1.887	1.813	1.825	1.829	2.194	2.201	2.189	2.592	2.624	2.615
O_5M_{41}	–	–	–	1.843	1.807	1.798	2.202	2.160	2.151	2.726	2.502	2.491
O_4M_{41}	1.872	1.844	1.819	–	–	–	–	–	–	–	–	–
$\angle S_3P_1O_{16}$	141.3	171.5	137.1	149.1	171.8	146.3	159.5	172.2	160.7	116.2	175.2	152.5
$\angle S_3P_1O_4$	100.4	94.1	53.8	102.9	97.3	45.7	106.1	99.3	56.8	104.3	92.0	53.4
$\angle S_3P_1O_5$	111.8	101.6	110.6	110.7	99.6	115.4	110.6	98.8	98.3	107.5	97.7	104.8
$\angle S_3P_1O_2$	98.2	92.0	68.1	96.8	88.0	77.1	93.7	87.1	76.9	103.9	94.9	72.8
$\angle S_3M_{40}O_4$	83.1	86.1	134.0	82.1	85.8	133.1	106.1	73.5	56.8	60.0	92.0	132.1
$\angle O_{16}M_{41}O_4$	144.6	98.1	80.6	–	–	–	–	–	–	–	–	–
$\angle O_5M_{41}O_{16}$	–	–	–	138.5	96.6	80.0	121.5	80.7	67.2	138.9	67.5	57.3
$\angle P_1O_{16}M_{41}$	39.8	78.4	88.8	42.4	78.0	86.1	52.0	84.3	90.3	39.1	90.2	92.6
$\angle P_1S_3M_{40}$	70.5	71.6	36.8	68.6	70.2	36.5	73.0	75.6	41.9	78.1	82.2	34.7
$\angle P_1O_{16}H_{24}$	162.1	104.1	114.2	161.1	103.8	116.0	157.2	100.3	113.3	163.3	98.7	110.1
$\angle M_{40}S_3C_{17}$	100.2	97.5	93.3	96.8	96.6	94.0	100.0	99.4	88.0	109.2	118.8	105.3
$\angle P_1S_3C_{17}$	104.2	107.3	128.0	105.1	107.1	109.1	106.0	107.9	93.7	108.8	112.7	137.9

Results and discussion

Phosphodiester bond in different chemical environments can be visualized in substrates (*1−4)* depicted in Fig. 1. Tp-ST *(1)* is comprised of phosphodiester bond where phosphate ion connects 3′-Thymidylyl and 5′-S-thymidine group; the leaving group in Tp-ST was systematically varied in (*2−4)* keeping the Tp moiety on 5′ side the same. As pointed out in the preceding section pathway **'A'** in Fig. 3 shows (two) metal ions bound to either S_3 or O_{16} and to O_4 of phosphoryl group. The present calculations clearly point out that during hydrolysis pentavalent phosphorus intermediate (local minimum) was not located. It was, therefore, inferred that the reaction follows A_ND_N mechanism comprised of a single step wherein nucleophile attack on P atom and leaving group departure occurs simultaneously. On the other hand, B3LYP/6–31++G (d,p) calculations on Thymidylyl (3′–5′) thymidine (Tp-OT) [37] follows (A_N+D_N) mechanism with an intermediate and the transition state on either side of it. In other words, substitution of sulfur at 5′ of sugar in Tp-OT alters the mechanistic pathway of hydrolysis reaction. It was pointed out in the preceding section that Tp-ST hydrolysis was carried out by simultaneously contraction and elongation of P_1O_{16} and P_1S_3 distances with step-size of 0.025 Å. A maximum on the energy profile thus obtained finally converged to a stationary point structure identified to be the transition state (TS), which consequently transforms to product. Yet another pathway **'B'** where metal ion interacts with phosphoryl group is displayed in Fig. 3. Here the metal ion bound to both O_4 as well as O_5 and to either hydroxyl group or 5′-S- thymidine oxygen on Tp-ST which engenders one transition state structure as also noticed for **'A'** pathway.

Optimized structures of reactant, TS and product in both **'A'** and **'B'** pathways are depicted in Fig. 4. Activation energies (E_A) and reaction energies (E_R) for these pathways are given in Table 1. An energy barrier for **'A'** pathway in lithium catalyzed phosphodiester hydrolysis (8.2 kcal mol^{-1}) turns out to be ~1.8 kcal mol^{-1} in excess than that for **'B'** pathway. On the other hand in Na and K catalyzed Tp-ST hydrolysis two pathways merge together and thus only **'B'** pathway becomes viable. As shown in Table 1 activation barrier of phosphodiester hydrolysis in presence of alkali metal turns out to be K (12.0 kcal mol^{-1}) > Na (9.5 kcal mol^{-1}) > Li (6.4 kcal mol^{-1}) along path **'B'**. Thus, hydrolysis rate follows the order: Li > Na > K. Corresponding energy profiles of **'A'** and **'B'** mechanisms in Tp-ST hydrolysis are displayed in Fig. 5. Selected geometrical parameters in reactant, product and TS incorporating Li are reported in Table 2. The P_1O_{16} bond distance predicted to be 2.391 Å for **'A'** pathway, which are longer compared to 2.358 Å along **'B'**. Thus bond formation seems to be larger in the TS along **'B'**. Further P_1S_3 separation that corresponds to bond breaking is 2.315 Å in **'A'** compared to 2.286 Å along profile **'B'**. In other words, bond cleavage is easier along **'A'**. Likewise comparison of $Li_{40}S_3$ bond distances in TS for **'A'** (2.360 Å) and **'B'** (2.409 Å) suggests closer approach of Li to phosphodiester. The cleavage of the 5′-S-thymidine is further evident from elongation of P_1O_4 and P_1O_5 bonds in TS along **'A'** as well as **'B'**. Bond distances and bond angles in stationary point structures of Na and K incorporated pathways are compared in Table 2. It should be remarked here that P_1O_{16} bond distances in TS along **'B'** pathway are: Li (2.358 Å) > Na (2.333 Å) > K (2.274 Å) while an opposite order has been predicted for P_1S_3 bond distances. Moreover $O_{16}P_1S_3$ bond angles turn out to be nearly linear and hence a transition state that possesses trigonal bipyramidal structure was attained along these profiles.

Atomic charges obtained from Hirshfeld population analysis in stationary point structures following **'A'** and **'B'** pathways are shown in Table 3. As can be noticed, phosphorus

Table 3 Hirshfeld charges on atomic centers of reactant, transition state and product along **'A'** and **'B'** pathways in Tp-ST hydrolysis incorporating alkali metal (Li, Na or K)

Atom	A			B								
	Li			Li			Na			K		
	R	TS	P	R	TS	P	R	TS	P	R	TS	P
P_1	0.530	0.524	0.585	0.541	0.525	0.590	0.514	0.512	0.557	0.496	0.508	0.545
O_2	−0.182	−0.172	−0.180	−0.188	−0.178	−0.197	−0.193	−0.185	−0.207	−0.186	−0.194	−0.203
S_3	−0.119	−0.215	−0.514	−0.125	−0.208	−0.485	−0.147	−0.236	−0.467	−0.168	−0.277	−0.478
O_4	−0.409	−0.419	−0.407	−0.411	−0.411	−0.388	−0.407	−0.410	−0.414	−0.426	−0.415	−0.426
O_5	−0.395	−0.394	−0.414	−0.385	−0.412	−0.433	−0.403	−0.414	−0.435	−0.412	−0.426	−0.448
O_{16}	−0.482	−0.371	−0.067	−0.485	−0.350	−0.055	−0.519	−0.388	−0.075	v0.551	−0.402	−0.112
H_{24}	0.090	0.107	0.200	0.085	0.109	0.203	0.057	0.085	0.191	0.045	0.078	0.176
M_{40}	0.327	0.423	0.556	0.328	0.429	0.546	0.423	0.508	0.623	0.459	0.572	0.688
M_{41}	0.382	0.348	0.239	0.373	0.323	0.267	0.463	0.418	0.385	0.500	0.461	0.430

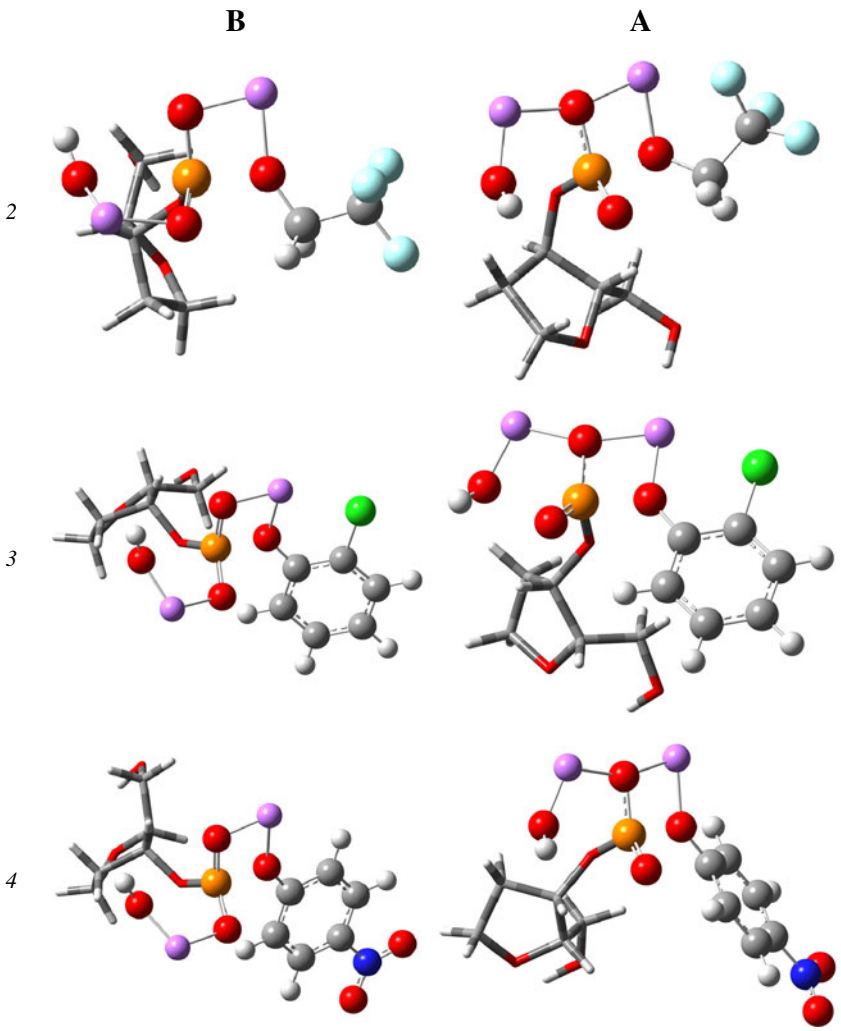

Fig. 6 Transition state structures along **'A'** and **'B'** in Li-catalyzed (*2–4)* hydrolysis

atom turns out to be largely electron deficient in pathway **'B'** while O_4 and O_5 atom centers are electron-rich. The TS along **'B'** reveals larger atomic charge on lithium than Na or K and hence it may be conjectured that P atom in TS for lithium catalyzed hydrolysis is more susceptible for hydroxyl ion attack and further strong electrostatic attractions between the electron deficient center (metal) and nucleophile bring about lowering of its activation barrier. Thus Tp-ST hydrolysis incorporating Li proceeds more rapidly than the remaining alkali metals.

As noticed in the case of Tp-ST hydrolysis of *2, 3* and *4* incorporating Li suggested both **'A'** and **'B'** pathways are viable unlike Na and K catalyzed hydrolysis for which only **'B'** pathway was characterized. Since the intermediate was

Table 4 Activation energies (E_A) and reaction energies (E_R) in kcal mol^{-1} along **'A'** and **'B'** pathways for metal (Li, Na or K) and Li(W), Na(W) and K(W) catalyzed (W representing water molecule) (*1–4*) hydrolysis

Substrates		A	B					
		Li	Li	Li(W)	Na	Na(W)	K	K(W)
1	E_A	8.2	6.4	11.9	9.5	16.7	12.0	17.2
	E_R	−11.0	−8.7	−33.4	−18.6	−9.7	−32.1	−9.9
2	E_A	5.7	5.6	7.3	6.9	12.3	12.7	15.3
	E_R	−43.1	−8.3	−4.0	−10.8	−7.0	−0.6	−23.2
3	E_A	5.0	4.8	6.8	6.5	8.6	10.3	14.8
	E_R	−19.0	−17.9	−23.4	−21.2	−28.2	−20.9	−12.1
4	E_A	4.2	3.9	3.1	6.2	5.4	9.1	8.4
	E_R	−24.0	−36.6	−30.4	−26.4	−29.9	−20.9	−30.1

Table 5 Atomic charges of reactant, transition state and product along **'A'** and **'B'** pathways in *(2−4)* hydrolysis incorporating alkali metal (Li, Na or K) from Hirshfeld population analysis

Substrates	Atom	A			B								
		Li			Li			Na			K		
		R	TS	P	R	TS	P	R	TS	P	R	TS	P
2	P_1	0.593	0.569	0.564	0.598	0.571	0.599	0.565	0.545	0.558	0.534	0.521	0.548
	O_2	−0.191	−0.187	−0.212	−0.192	−0.185	−0.183	−0.205	−0.194	−0.208	−0.208	−0.202	−0.199
	O_3	−0.384	−0.252	−0.429	−0.210	−0.239	−0.452	−0.216	−0.244	−0.453	−0.209	−0.250	−0.465
	O_4	−0.409	−0.428	−0.399	−0.424	−0.424	−0.389	−0.427	−0.434	−0.416	−0.428	−0.445	−0.434
	O_5	−0.384	−0.391	−0.432	−0.388	−0.414	−0.430	−0.410	−0.428	−0.436	−0.422	−0.449	−0.444
	O_{16}	−0.488	−0.388	−0.039	−0.479	−0.387	−0.059	−0.512	−0.403	−0.078	−0.546	−0.390	−0.092
	H_{24}	0.090	0.104	0.198	0.087	0.104	0.203	0.059	0.082	0.190	0.045	0.079	0.183
	M_{40}	0.449	0.416	0.317	0.444	0.497	0.293	0.594	0.568	0.409	0.536	0.498	0.473
	M_{41}	0.325	0.425	0.297	0.339	0.413	0.542	0.434	0.501	0.622	0.477	0.576	0.644
3	P_1	0.592	0.577	0.582	0.603	0.584	0.593	0.575	0.560	0.565	0.554	0.546	0.548
	O_2	−0.186	−0.180	−0.192	−0.193	−0.178	−0.196	−0.203	−0.195	−0.195	−0.193	−0.194	−0.200
	O_3	−0.191	−0.215	−0.386	−0.19	−0.216	−0.386	−0.189	−0.209	−0.381	−0.193	−0.225	−0.396
	O_4	−0.406	−0.425	−0.419	−0.421	−0.413	−0.391	−0.426	−0.421	−0.411	−0.448	−0.440	−0.434
	O_5	−0.400	−0.400	−0.407	−0.386	−0.400	−0.432	−0.402	−0.418	−0.431	−0.422	−0.419	−0.443
	O_{16}	−0.488	−0.404	−0.054	−0.482	−0.410	−0.056	−0.513	−0.415	−0.073	−0.516	−0.424	−0.089
	H_{24}	0.088	0.101	0.206	0.086	0.098	0.202	0.058	0.079	0.192	0.054	0.074	0.185
	M_{40}	0.439	0.423	0.290	0.422	0.396	0.287	0.520	0.476	0.387	0.587	0.557	0.474
	M_{41}	0.327	0.417	0.558	0.339	0.409	0.549	0.434	0.501	0.587	0.494	0.565	0.647
4	P_1	0.593	0.581	0.581	0.605	0.589	0.588	0.573	0.569	0.564	0.552	0.553	0.548
	O_2	−0.183	−0.177	−0.192	−0.187	−0.179	−0.191	−0.185	−0.183	−0.192	−0.188	−0.197	−0.202
	O_3	−0.200	−0.224	−0.396	−0.202	−0.216	−0.363	−0.207	−0.221	−0.385	−0.197	−0.222	−0.395
	O_4	−0.411	−0.425	−0.425	−0.427	−0.414	−0.414	−0.429	−0.418	−0.420	−0.430	−0.417	−0.437
	O_5	−0.389	−0.383	−0.400	−0.377	−0.390	−0.408	−0.389	−0.393	−0.418	−0.420	−0.421	−0.441
	O_{16}	−0.487	−0.416	−0.046	−0.477	−0.425	−0.054	−0.520	−0.430	−0.082	−0.504	−0.460	−0.087
	H_{24}	0.089	0.100	0.210	0.089	0.096	0.191	0.058	0.076	0.189	0.053	0.067	0.185
	M_{40}	0.555	0.529	0.395	0.539	0.514	0.423	0.626	0.597	0.495	0.571	0.551	0.553
	M_{41}	0.327	0.413	0.564	0.344	0.404	0.342	0.421	0.496	0.633	0.476	0.555	0.653

not identified along the reaction pathway it was predicted catalysis of (*2−4)* has been facilitated via A_ND_N mechanism. Transition state structure for *2, 3* and *4* incorporating Li catalyst in **'B'** and **'A'** pathways are shown in Fig. 6. Selected geometrical parameters of reactant, product and transition state incorporating Li, Na and K are presented in Tables 1S through Table 3S of supporting information. Energy barrier values given in Table 4 reveal that alkali metal catalyzed hydrolysis rates follow the same order as inferred in the case of Tp-ST hydrolysis. Furthermore Tp-ST analogues involving aryl leaving groups *3* and *4* hydrolyzed faster than Tp-ST and *2* which are evident from activation energy barrier data reported in Table 4. It should be remarked here that extended conjugation from NO_2 group attached to phenyl moiety in *4* stabilizes the transition state along its hydrolysis pathway consequently lowering the activation barrier as shown in Table 4.

To gauge the perturbation around central P atom in these Tp-ST derivatives we carried out Hirshfeld population analysis. Atomic charges in stationary point structures following **'A'** and **'B'** pathways in these substrates incorporating Li, Na and K are given in Table 5. Thus, *4* reveals most electron-deficient central P making it more susceptible for the nucleophile attack and thus yields low energy of activation (3.9 kcal mol^{-1}) along **'B'** pathway for Li catalyzed hydrolysis.

It may be remarked here that generally biological reactions are facilitated by the presence of solvent (water). To understand how hydration influences complexation properties of alkali metals we carried out the B3LYP calculations on model systems wherein each metal ion is bound to one water molecule. The present calculations reveal that the mechanistic pathway of phosphodiester hydrolysis follows a single step (A_ND_N) mechanism as also inferred for gas phase reactions. Optimized structure of reactant, transition state and product during hydrolysis of phosphodiester bond in substrates (*1–4*) are shown in Fig. 7. Activation energies thus obtained are compared with those from gas phase in Table 4. It may readily be noticed that the presence of solvent reveals the activation barrier follows the order: Tp-OPh(p-NO_2) < Tp-OPh(o-Cl) < Tp-OCH_2CF_3 < Tp-ST, in accordance with the trend inferred from the gas phase calculations.

Structural parameters in stationary point geometries along ***'B'*** pathway thus obtained (Li(W), Na(W) and K (W) denote hydrated metal ions) in (*1−4)* are reported in Table 4S through Table 7S of supporting information. It may readily be noticed that the P_1O_{16} distance (that refers to bond formation) in hydrolysis incorporating hydrated metal ion follows the order: *1*(1.854) < *2*(2.274) < *3*(2.313) < *4* (2.369), which suggests that closer approach of hydroxyl ion

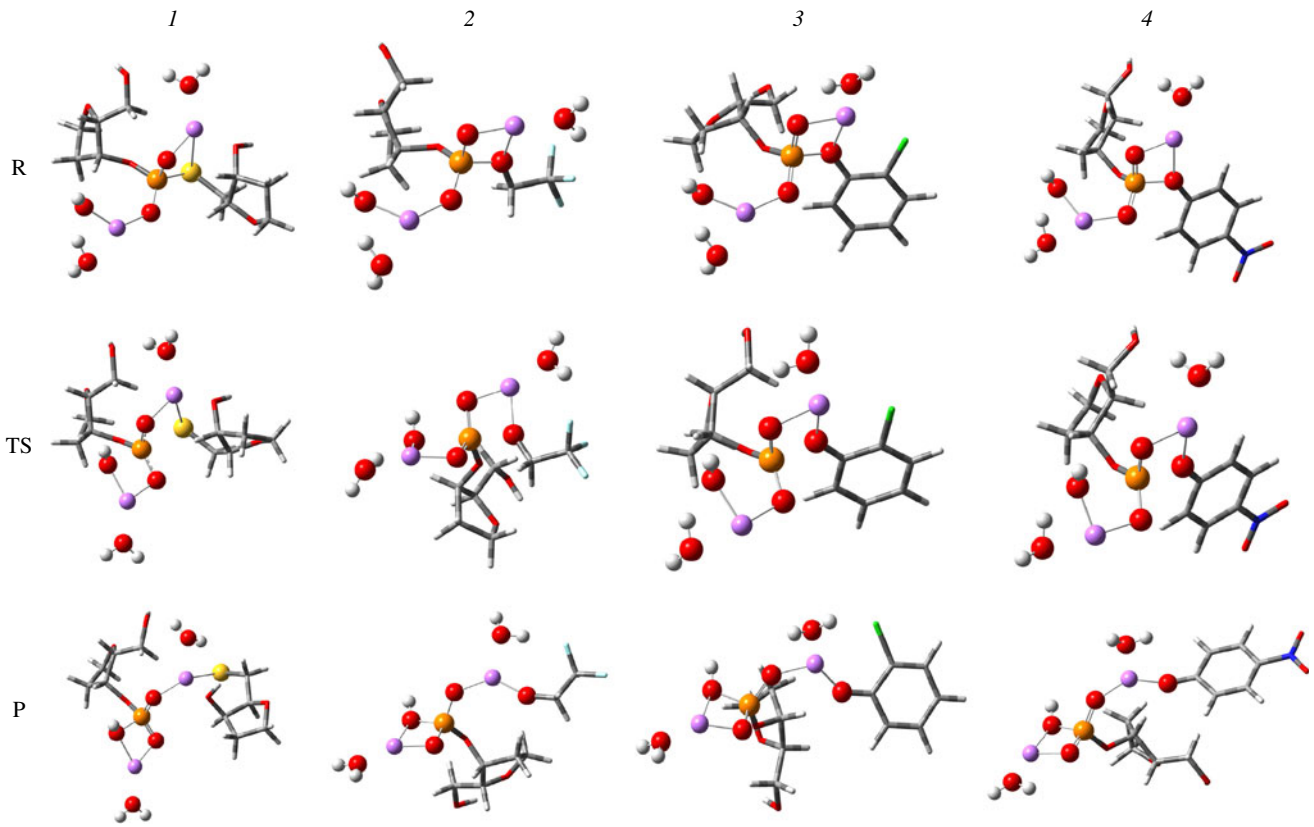

Fig. 7 Stationary point structures on reaction pathway for (*1−4)* hydrolysis catalyzed by Li(W)

in substrate *1* results in larger activation barrier than the remaining substrates (*2*−*4*).

As may readily be noticed unlike in the case of substrate *4*, activation energies of phosphodiester hydrolysis incorporating a hydrated metal ion of (*1*–*3*) turn out to be ~2 kcal mol^{-1} to 7 kcal mol^{-1} larger than corresponding gas phase values. Lowering of activation energy in the case of *4* results from conjugation from p-NO_2 functionality which renders relatively large stability to its transition state facilitating easier cleavage of P_1O_3 bond. Activation barrier of phosphodiester hydrolysis stems from perturbation around phosphate group in the substrate. We therefore, obtain net atomic charges in stationary point geometries of (*1*−*4*). Hirshfeld atomic charges accompanying phosphodiester hydrolysis in the presence of bare metal as well as hydrated metal ion (M(W)) are given in Table 6. It may be remarked that in the presence of metal bound to water molecule O_3 atom turns out to be relatively electron deficient compared to gas phase which results in weakening of P_1O_3bond.

Conclusions

Systematic analyses of mechanistic pathways of alkali metal (Li, Na, K) catalyzed hydrolysis of Tp-ST and its derivatives *2, 3* and *4* have been carried out within the B3LYP/6–31++G(d,p) framework of theory. Contrary to Tp-OT hydrolysis [37] which revealed (A_N+D_N) mechanism, substitution of 5′ sugar either by sulfur (as in Tp-ST) or by alkyl/aryl substituent (*2*–*4*) alters the reaction pathway. In other words Tp-ST and its derivatives facilitate hydrolysis via A_ND_N mechanism in which bond making and bond breaking occur in a

Table 6 Hirshfeld atomic charges in transition state along phosphodiester hydrolysis in (1−*4*) incorporating bare metal (Li, Na or K) and hydrated metal (Li(W), Na(W) and K(W) ions)

Substrates		Li	Li(W)	Na	Na(W)	K	K(W)
1	P_1	0.525	0.540	0.512	0.517	0.508	0.507
	O_2	−0.178	−0.182	−0.185	−0.187	−0.194	−0.187
	S_3	−0.208	−0.359	−0.236	−0.249	−0.277	−0.302
	O_4	−0.411	−0.404	−0.410	−0.399	−0.415	−0.426
	O_5	−0.412	−0.419	−0.414	−0.371	−0.426	−0.425
	O_{16}	−0.350	−0.165	−0.388	−0.395	−0.402	−0.239
	M_{40}	0.323	0.362	0.508	0.325	0.572	0.416
	M_{41}	0.429	0.190	0.418	0.423	0.461	0.548
2	P_1	0.571	0.561	0.545	0.552	0.521	0.499
	O_2	−0.185	−0.187	−0.194	−0.192	−0.202	−0.202
	O_3	−0.239	−0.240	−0.244	−0.364	−0.250	−0.262
	O_4	−0.424	−0.425	−0.434	−0.420	−0.445	−0.459
	O_5	−0.414	−0.425	−0.428	−0.416	−0.449	−0.453
	O_{16}	−0.387	−0.263	−0.403	−0.126	−0.390	−0.213
	M_{40}	0.497	0.335	0.568	0.341	0.498	0.450
	M_{41}	0.413	0.342	0.501	0.508	0.576	0.542
3	P_1	0.584	0.573	0.560	0.552	0.546	0.527
	O_2	−0.178	−0.191	−0.195	−0.195	−0.194	−0.193
	O_3	−0.216	−0.225	−0.209	−0.218	−0.225	−0.233
	O_4	−0.413	−0.408	−0.421	−0.421	−0.440	−0.438
	O_5	−0.400	−0.412	−0.418	−0.425	−0.419	−0.434
	O_{16}	−0.410	−0.271	−0.415	−0.253	−0.424	−0.246
	M_{40}	0.396	0.276	0.476	0.360	0.557	0.444
	M_{41}	0.409	0.349	0.501	0.468	0.565	0.530
4	P_1	0.589	0.578	0.569	0.558	0.553	0.550
	O_2	−0.179	−0.190	−0.183	−0.197	−0.197	−0.197
	O_3	−0.216	−0.208	−0.221	−0.214	−0.222	−0.212
	O_4	−0.414	−0.407	−0.418	−0.414	−0.417	−0.425
	O_5	−0.390	−0.398	−0.393	−0.409	−0.421	−0.420
	O_{16}	−0.425	−0.296	−0.430	−0.281	−0.460	−0.285
	M_{40}	0.514	0.328	0.597	0.434	0.551	0.519
	M_{41}	0.404	0.345	0.496	0.466	0.555	0.545

single reaction step. Activation barrier for hydrolysis of (*1*−*4*) incorporating potassium turns out to be larger than those with sodium and lithium. Moreover, the reaction rate in Tp-ST is predicted to be slower than that of *4*. The hydrolysis rate is predicted to follow the order: Tp-OPh(p-NO_2) > Tp-OPh(O-Cl) > Tp-OCH_2CF_3 > Tp-ST in the presence of bare metal ion as well as metal ion bound to water molecule. The substrates possessing an aryl leaving group reveal lower activation barrier than Tp-ST (*1*).

Acknowledgments S.P.G. is grateful to the University Grants Commission (UGC), New Delhi, India (Research Project F34-370/2008 (SR)) and to the University of Pune for disbursing the research grant under the potential excellence (UPE) scheme. We thank the Center for Network Computing, University of Pune, for providing computational facilities.

References

1. More O'Ferrall RA (1970) J Chem Soc B 0:274–277
2. Jencks WP (1985) Chem Rev 85:511–527
3. Dejaegere A, Lim C, Karplus M (1991) J Am Chem Soc 113:4353–4355
4. Lim C, Karplus M (1990) J Am Chem Soc 112:5872–5873
5. Lim C, Tole P (1992) J Phys Chem 96:5217–5219
6. Tole P, Lim C (1993) J Phys Chem 97:6212–6219
7. Tole P, Lim C (1994) J Am Chem Soc 116:3922–3931
8. Chang NY, Lim C (1998) J Am Chem Soc 120:2156–2167
9. Uchimaru T, Tanabe K, Nishikawa S, Taira K (1991) J Am Chem Soc 113:4351–4353
10. Westheimer FH (1981) Chem Rev 4:313–326
11. Hengge AC, Cleland WW (1990) J Am Chem Soc 112:7421–7422
12. Admiraal SJ, Herschlag D (1995) Chem Biol 2:729–739
13. Takeda N, Shibata M, Tajima N, Hirao K, Komiyama M (2000) J Org Chem 65:4391–4396
14. Yatsimirsky AK (2005) Coord Chem Rev 249:1997–2011
15. Morrow JR, Iranzo O (2004) Curr Opin Chem Biol 8:192–200
16. Morales-Rojas H, Moss RA (2002) Chem Rev 102:2497–2522
17. Liu C, Wang M, Zhang T, Sun H (2004) Coord Chem Rev 248:147–168
18. Brown RS, Neverov AA (2002) J Chem Soc Perkin Trans 2:1039–1049
19. Williams NH (2004) Biochim Biophys Acta 1697:279–287
20. Molenveld P, Engbersen JFJ, Reinhoudt DN (2000) Chem Soc Rev 29:75–86
21. Kramer R (1999) Coord Chem Rev 182:243–261
22. Williams NH, Takasaki B, Wall M, Chin J (1999) Acc Chem Res 32:485–493
23. Lim S, Franklin SJ (2004) Cell Mol Life Sci 61:2184–2188
24. Schneider HJ, Yatsimirsky AK (2003) Metal ions in biological systems. In: Sigel A, Sigel H (eds) Lanthanide catalyzed hydrolysis of phosphate esters and nucleic acids, vol 40. Dekker, New York, pp 369–462
25. Franklin SJ (2001) Curr Opin Chem Biol 5:201–208
26. Komiyama M, Takeda N, Shigekawa H (1999) Chem Commun 16:1443–1451
27. Blasko A, Bruice TC (1999) Acc Chem Res 32:475–484
28. Suelter CH (1970) Science 168:789–795
29. Suelter CH (1974) Metal ions in biological systems. In: Sigel A, Sigel H (eds) Monovalent cations in enzyme-catalyzed reactions, vol 3. Marcel Dekker, New York, pp 201–251
30. Phillips RS, Chen HY, Shim D, Lima S, Tavakoli K, Sundararaju B (2004) Biochem 43:14412–14419
31. Zhang R, Villeret V, Lipscomb WN, Fromm HJ (1996) Biochemistry 35:3038–3043
32. O'Brien MC, McKay DB (1995) J Biol Chem 270:2247–2250
33. Wilbanks SM, McKay DB (1995) J Biol Chem 270:2251–2257
34. Zhang R, Villeret V, Lipscomb WN, Fromm HJ (1996) Biochemistry 35:3038–3043
35. Kamerlin SCL, Wilkie J (2007) Org Biomol Chem 5:2098–2108
36. Pinjari RV, Kaptan SS, Gejji SP (2009) Phys Chem Chem Phys 11:5253–5262
37. Rahimian M, Gejji SP (2012) Computational and Theoretical Chemistry 984:57–67
38. Tagle PG, Zúñiga IV, Taran O, Yatsimirsky AK (2006) J Org Chem 1:9713–9722
39. Becke AD (1993) J Chem Phys 98:5648–5652
40. Lee C, Yang W, Parr RG (1988) J Phys Rev B Condens Matter Mater Phys 37:785–789
41. Frisch MJ, Trucks GW, Schlegel HB, Scuseria GE et al (2009) Gaussian 09. Gaussian Inc, Wallingford
42. Sousa SF, Fernandes PA, Ramos MJ (2007) J Phys Chem A 111:10439–10452
43. Hirshfeld FL (1977) J Theor Chim Acta 44:129–138
44. Davidson ER, Chakravorty SC (1992) J Theor Chim Acta 83:319–330